Comparison of Four Different Energy Balance Models for Estimating Evapotranspiration in the Midwestern United States

Ramesh K. Singh [1],* and Gabriel B. Senay [2]

[1]   ASRC Federal InuTeq, Contractor to the U.S. Geological Survey (USGS) Earth Resources Observation and Science (EROS) Center, 47914 252nd Street, Sioux Falls, SD 57198, USA

[2]   USGS EROS Center, North Central Climate Science Center, Colorado State University, Fort Collins, CO 80523, USA; senay@usgs.gov

*   Correspondence: rsingh@usgs.gov; Tel.: +1-605-594-2751; Fax: +1-605-594-6529

Abstract: The development of different energy balance models has allowed users to choose a model based on its suitability in a region. We compared four commonly used models—Mapping EvapoTranspiration at high Resolution with Internalized Calibration (METRIC) model, Surface Energy Balance Algorithm for Land (SEBAL) model, Surface Energy Balance System (SEBS) model, and the Operational Simplified Surface Energy Balance (SSEBop) model—using Landsat images to estimate evapotranspiration (ET) in the Midwestern United States. Our models validation using three AmeriFlux cropland sites at Mead, Nebraska, showed that all four models captured the spatial and temporal variation of ET reasonably well with an R^2 of more than 0.81. Both the METRIC and SSEBop models showed a low root mean square error (<0.93 mm· day^{-1}) and a high Nash–Sutcliffe coefficient of efficiency (>0.80), whereas the SEBAL and SEBS models resulted in relatively higher bias for estimating daily ET. The empirical equation of daily average net radiation used in the SEBAL and SEBS models for upscaling instantaneous ET to daily ET resulted in underestimation of daily ET, particularly when the daily average net radiation was more than 100 W· m^{-2}. Estimated daily ET for both cropland and grassland had some degree of linearity with METRIC, SEBAL, and SEBS, but linearity was stronger for evaporative fraction. Thus, these ET models have strengths and limitations for applications in water resource management.

Keywords: comparison; evapotranspiration; METRIC; SEBAL; SEBS; SSEBop; Landsat; remote sensing

1. Introduction

Modeling evapotranspiration (ET), the combined loss of water from soil through evaporation and from vegetation through transpiration, has many applications in agricultural management [1,2], carbon sequestration [3,4], climate modeling [5], drought monitoring [6], energy security [7], hydrological modeling [8], irrigation scheduling [9], and watershed development [10,11]. Various models and techniques are used for accurately estimating ET at field to global scales. Many techniques such as lysimeters, sap flow, eddy covariance method, Bowen ratio system, and scintillometer are accurate and efficient but cannot be used for regional-to-global scale ET mapping due to prohibitive cost and logistical limitations.

The availability of no-cost satellite images, advances in computing technology, and affordability of computing resources has allowed the development and use of remotely sensed images for water use estimation. Remotely sensed images are increasingly used for estimating ET at different temporal and spatial scales. During the last two decades, many models were developed for estimating land surface

evapotranspiration using remotely sensed data [12–14]. Some of these models include SEBAL (Surface Energy Balance Algorithm for Land) [15,16], SEBS (Surface Energy Balance System) [17], METRIC (Mapping EvapoTranspiration at high Resolution with Internalized Calibration) [18], and SSEBop (Operational Simplified Surface Energy Balance) models [19,20]. The SEBAL model has been widely used under different climatic conditions at both field and catchment scales with a typical accuracy of 85% at field scale on a daily basis and increasing to 95% on a seasonal basis [21]. Application of the SEBS model over 20 FLUXNET sites encompassing grassland, cropland, shrubland, evergreen needleleaf forest, and deciduous broadleaf forest showed promising results with the Nash–Sutcliffe efficiency (NSE) and the root mean squared difference (RMSD) of 0.42 and 84 W·m^{-2}, respectively [22]. Use of the METRIC model over an irrigated cotton field in Maricopa, Arizona, at fine and moderate spatial scales showed an RMSD of less than 1.9 mm·day^{-1}, and METRIC was preferred when model ancillary data were sparse [23]. The SSEBop model-based estimation of ET in the Colorado River Basin with diverse ecosystems and complex hydro-climatic regions nicely captured the variability in annual ET with an overall coefficient of determination (R^2) of 0.78 and a mean bias error of about 10%. Thus, all of these models used by different research groups have worked well in different areas. However, selecting a model for estimating ET from many available energy balance models is challenging as each model has its strengths and limitations like any other modeling approaches.

Comparison of different models for estimating reference/potential ET has helped users and researchers in standardizing and identifying the best model for specific regions and climatic conditions [1,24–26]. Similarly, comparison of different models for estimating actual ET provides important information on suitability and limitations of models to users and developers. These comparisons help users understand the strength/limitations of different techniques and better understand the uncertainties in various model components and their impacts on final ET values [2]. Different models for ET estimation have different input data requirements and influence the model selection based on input data availability. In addition, the source of input data may also influence the model performance based on the quality and accuracy of the input data. Comparison of three energy balance models using measured values of net radiation (R_n) and soil heat flux (G) showed comparable results but inter-model discrepancies are likely to be greater if the model estimates of R_n and G are used [27]. The complexities of various models are different and affect the ease of model set-up and operational efficiency. Research has shown that added complexities do not necessarily lead to improved performance of hydrological models [28]. Performance of ET models may also vary seasonally depending upon rainfall distribution. The SEBAL model gave comparable results to the water balance method during the rainy season but a higher value during the dry season [29]. Another study on the comparison of methods for estimating forest evapotranspiration showed the effects of severe surface dryness and rainfall events [30]. Comparison of a radiometric surface temperature-based energy balance model and reflectance-based vegetation indices model have shown that the later model may be less sensitive to detecting crop water stress and estimating ET until there is actual reduction in biomass or changes in canopy geometry [27,31].

Based on the literature, it is evident that models may have overall high performance, but there are substantial differences in capturing the spatial and temporal variability of ET under diverse agro-hydro-climatic conditions, thus highlighting the need for further improvement and validation [32]. The objective of this study is to compare four commonly used ET models—Mapping EvapoTranspiration at high Resolution with Internalized Calibration (METRIC) model, Surface Energy Balance Algorithm for Land (SEBAL) model, Surface Energy Balance System (SEBS) model, and Operational Simplified Surface Energy Balance (SSEBop) model—using 2001 Landsat images to estimate ET in the Midwestern United States.

2. Materials and Methods

2.1. Study Area

This study was conducted in the Midwestern United States in a relatively flat plain dominated by croplands, mainly maize and soybean fields. We used Landsat satellite images (path 28, row 31) acquired on 4 July, 5 August, 24 October, and 11 December (Landsat 5, Thematic Mapper: TM) and four images acquired on 13 August, 29 August, 30 September, and 16 October (Landsat 7, Enhanced Thematic Mapper Plus: ETM+) during the 2001 crop growing season (Figure 1). The Landsat images were processed using Erdas Imagine software (Hexagon Geospatial Inc., Norcross, GA, USA) based on standard procedure where digital number values are first converted to radiance and then to reflectance [20]. The University of Nebraska Agricultural Research and Development Center (ARDC) near Mead, Nebraska, within the Landsat scene footprint has three eddy covariance (EC) measurements sites. These three sites are Mead Site 1: center-pivot irrigated continuous maize (41°9′54.2″ N, 96°28′35.9″ W, 361 m above mean sea level, area 48.7 ha); Mead Site 2: center-pivot irrigated maize-soybean rotation (41°9′53.5″ N, 96°28′12.3″ W, 362 m above mean sea level, area 52.4 ha); and Mead Site 3: rainfed maize–soybean rotation (41°10′46.8″ N, 96°26′22.7″ W, 362 m above mean sea level, area 65.4 ha). Only maize was grown at all three sites under no-till management during the 2001 crop growing season employing the best management practices. Maize was planted on 10 May, 11 May, and 14 May and harvested on 18 October, 22 October, and 29 October, respectively, at Mead Sites 1–3. The fluxes were measured using an omnidirectional 3D sonic anemometer (Model R3: Gill Instruments Ltd., Lymington, UK), a closed-path infrared CO_2/H_2O gas analyzing system (Model LI6262: Li-Cor Inc., Lincoln, NE, USA), and a krypton hygrometer (Model KH20: Campbell Scientific, Logan, UT, USA). Additional details about the sites, installation, operation and maintenance of the EC tower, data processing, and quality control are given elsewhere [33].
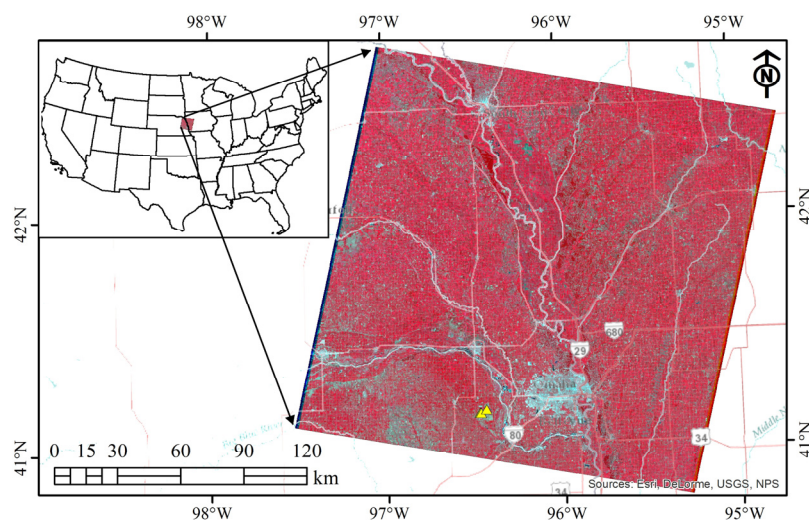

Figure 1. Location map of the study area for Landsat path 28, row 31. Eddy covariance sites are also shown using yellow triangles just southwest of Omaha, Nebraska, (blue-gray color) in the lower middle part of the image.

2.2. Energy Balance Models

We provide a brief overview of the models used in this study, and full details of the models are provided in their respective references. A brief overview of data used in this study is provided in Table 1.

Table 1. Overview of datasets used in this study.

No.	Dataset	Symbol	Source	Resolution
1	Elevation	z	DEM	30 m
2	Surface temperature	T_s	Landsat	60/120 m
3	Normalized Difference Vegetation Index	-	Landsat	30 m
4	Albedo	α	Landsat	30 m
5	Momentum roughness length	Z_{om}	NDVI	30 m
6	Temperature difference	dT	Model	1 km
7	Flux ET	-	Eddy covariance	-
8	Extraterrestrial solar radiation	R_a	Model	-
9	Alfalfa reference ET	ET_r	Weather station	-
10	Grass reference ET	ET_o	GDAS	10 km

2.2.1. The METRIC Model

The METRIC model, a variant of the SEBAL model, estimates ET as a residual of the surface energy balance equation:

$$LE = R_n - G - H \tag{1}$$

where LE is latent heat flux (W·m^{-2}) consumed for ET, R_n is net radiation (W·m^{-2}), G is soil heat flux (W·m^{-2}), and H is sensible heat flux (W·m^{-2}).

The innovative aspect of the METRIC model is that it uses weather-based reference ET, thus using ground-based reference ET to tie down satellite-based actual ET. In addition, use of daily water balance to compute ET at a hot anchor pixel helps to account for the residual soil moisture content.

ET at each pixel at the time of satellite overpass is calculated as

$$ET_{ins} = 3600 \times \frac{LE}{\lambda \times \rho_w} \tag{2}$$

where ET_{ins} is instantaneous ET (mm·h^{-1}), λ is latent heat of vaporization (J·kg^{-1}), and ρ_w is density of water (kg·m^{-3}).

The reference ET fraction (ET_rF) is computed as

$$ETrF = \frac{ET_{ins}}{ET_r} \tag{3}$$

where ET_r is tall grass (alfalfa) reference ET (mm·h^{-1}) at the time of satellite overpass calculated from data collected at a nearby weather station. It is assumed that the ET_rF computed for the time of satellite overpass is the same as the ET_rF over the 24-h average.

Finally, daily ET (ET_{24}) at each pixel is computed as

$$ET_{24} = ETrF \times ET_{r\_24} \tag{4}$$

where ET_{r_24} is the cumulative 24-h daily ET_r (mm·day^{-1}) using the standardized ASCE (American Society of Civil Engineers) Penman–Monteith equation for the day of satellite image acquisition. More details about the METRIC model can be found in [2,18].

2.2.2. SEBAL Model

The SEBAL model, a physically based multi-step surface energy balance model, provided a pioneering approach for land surface parameterization based on near-surface vertical air temperature difference. This vertical temperature difference (dT) between aerodynamic surface temperature and air temperature was assumed to be linearly related to the remotely sensed radiometric surface temperature. This approach excluded the need for independent synoptic air temperature observations for a correct

physical coupling between the surface roughness for heat transport, vertical temperature gradient, and fluxes [16]. This *dT* parameterization also alleviated the need for accurate estimation of radiometric surface temperature due to uncertainty caused by atmospheric attenuation, radiometric calibration, and contamination [2].

Based on *Rn*, *G*, and *H* computations at the time of satellite overpass, the evaporative fraction (EF) at each pixel of the image is computed as

$$EF = \frac{R_n - G - H}{R_n - G} \tag{5}$$

The EF computed for the time of satellite overpass is assumed to be constant over the 24-h period for the day of image acquisition. Thus, daily ET at each image pixel is calculated as

$$ET_{24} = \frac{8.64 \times 10^7 \times EF \times (R_{n24} - G_{24})}{\lambda \times \rho_w} \tag{6}$$

where R_{n24} is daily average net radiation (W·m^{-2}), the difference between incoming net shortwave radiation and outgoing net longwave radiation, and G_{24} is daily average soil heat flux (W·m^{-2}) usually assumed to be zero for soil and vegetation surfaces. R_{n24} is computed as

$$R_{n24} = (1 - \alpha) \times R_a \times \tau_{sw} - 110 \times \tau_{sw} \tag{7}$$

where R_a is daily extraterrestrial solar radiation (W·m^{-2}), and τ_{sw} is daily atmospheric transmittance affected by dust, humidity, and other pollutants in the air. More details about the SEBAL model can be obtained from [2,16,21].

2.2.3. SEBS Model

The SEBS model is another physically based energy balance model that does not require any *a priori* knowledge of the actual turbulent heat fluxes. The model uses energy balance at wet and dry limiting conditions to compute instantaneous relative evaporation (Λ_r) as

$$\Lambda_r = 1 - \frac{H - H_{wet}}{H_{dry} - H_{wet}} \tag{8}$$

where H_{wet} is sensible heat flux (W·m^{-2}) under the wet limiting condition where ET takes place at potential rate, and H_{dry} is sensible heat flux (W·m^{-2}) at the dry limiting condition where ET is zero due to limited soil moisture.

The daily evaporative fraction is formulated as

$$\Lambda = \frac{\Lambda_r \times LE_{wet}}{R_n - G} \tag{9}$$

Finally, the daily ET is computed as

$$ET_{24} = \frac{8.64 \times 10^7 \times \Lambda \times (R_{n24} - G_{24})}{\lambda \times \rho_w} \tag{10}$$

Additional details on the SEBS model are provided by [17,34]. The SEBS model consists of a set of tools for determining land surface parameters including roughness length for heat transfer for estimating evaporative fraction and ET based on energy balance at limiting cases [17].

2.2.4. SSEBop Model

The SSEBop model is based on a simplified surface energy balance principle that does not solve for *H* explicitly like METRIC, SEBAL, and SEBS, as these three models use the Monin–Obukhov Similarity theory for stability correction functions for momentum and sensible heat transfer. The innovative aspect of the SSEBop model is that it is based on a predefined differential temperature *dT* to define two extreme limiting surface temperatures: Cold temperature (T_c) in case of little or no sensible heat flux and hot temperature (T_h) in case of little or no latent heat flux. The innovative parameterization procedure for hot and cold limiting conditions eliminated the subjectivity that could be introduced during the manual hot and cold reference selection.

The ET fraction (ET_f) is computed as

$$ET_f = \frac{T_h - T_s}{dT} \tag{11}$$

where T_h is idealized reference hot pixel temperature (K), T_s is radiometric land surface temperature (K), and *dT* is predefined temperature difference between hot and cold reference conditions that is representative of temperature difference between bare dry surface and air. The T_c is estimated from the daily maximum air temperature, and T_h is then calculated as the sum of T_c and *dT*.

The daily ET is calculated as

$$ET_{24} = ET_f \times k \times ET_0 \tag{12}$$

where ET_o is short grass reference ET (mm· day^{-1}) and *k* is a scaling coefficient based on calibration (here we used *k* as 1). Additional details on the SSEB$_{op}$ model can be obtained from [19,20].

2.3. Models Validation

We estimated actual ET based on the METRIC, SEBAL, SEBS, and SSEBop models using Landsat images acquired on eight dates. The estimated ET for the pixel that has a flux tower was compared with the eddy covariance measurements (Level 4: gapfilled and adjusted data) at three sites discussed in Section 2.1. Validation of the estimated ET was done by comparing estimated ET for the pixel located at the flux tower site with that of flux tower actual measurement of ET. We have three flux tower sites; thus for eight satellite overpass dates, we have 24 (8 × 3) pairs of data for validation. We used different statistical measures to evaluate the model performance at the validation sites. These statistical measures included Pearson's correlation coefficient (*r*), coefficient of determination (R^2), relative error (RE), root mean square error (RMSE), mean bias error (MBE), mean absolute error (MAE), and Nash–Sutcliffe's efficiency (NSE). It was assumed that any discrepancies between observed and estimated ET is due to error in estimated ET. However, in reality, there are also uncertainties associated with the eddy covariance measurements due to instrument sampling error, source area, failure to account for all the mechanisms of aerodynamic transport of energy, and other random observation errors. Additional details on these issues can be found in [22,35].

3. Results and Discussion

3.1. Spatial and Temporal Variation of ET Using the METRIC Model

The ET map based on the METRIC model showed the spatial and temporal variation of ET within the study area (Figure 2). As expected, ET was higher during the growing season than during the non-growing season. The urban area (Omaha, NE, USA) in the lower middle part of the image can be seen distinctly in the first four ET maps, but not in the last four ET maps due to the lower ET of urban areas as compared to the surrounding agricultural and natural vegetated areas. ET was also higher for the river and riparian areas along the river compared to other areas. In general, ET was high over the study area on 4 July 2001 due to higher residual moisture content from a previous precipitation event. Table 2 shows the evaporation coefficient (K_e) for the hot pixel based on soil water balance

run on a daily basis. K_e was also high on 24 October 2001 but its effect on ET in the study area was minimal due to a localized precipitation event. High residual moisture content of the hot pixel may cause underestimation of sensible heat flux at the anchoring pixels in the conventional METRIC model, thus, increasing the uncertainty of the estimated ET [36].

Alfalfa-based reference ET (ET_r) is used in the METRIC model for calibrating the energy balance functions and upscaling the instantaneous ET to daily ET. ET in many irrigated fields in arid and semiarid regions can exceed net radiation due to advection effects. Use of ET_r in the METRIC model helps to compensate to certain extent for regional advection [2,36].

Selection of hot and cold pixels in the METRIC model is important for accurate estimation of ET. The hot pixel is generally selected from a dry, bare agricultural field that does not necessarily have the highest T_s value. Similarly, the cold pixel is selected from well-watered and fully covered vegetation representative of the agricultural area. Thus, the METRIC model, like other models requiring selection of hot and cold pixels, relies on the user's ability to select appropriate anchoring pixels [2,37].
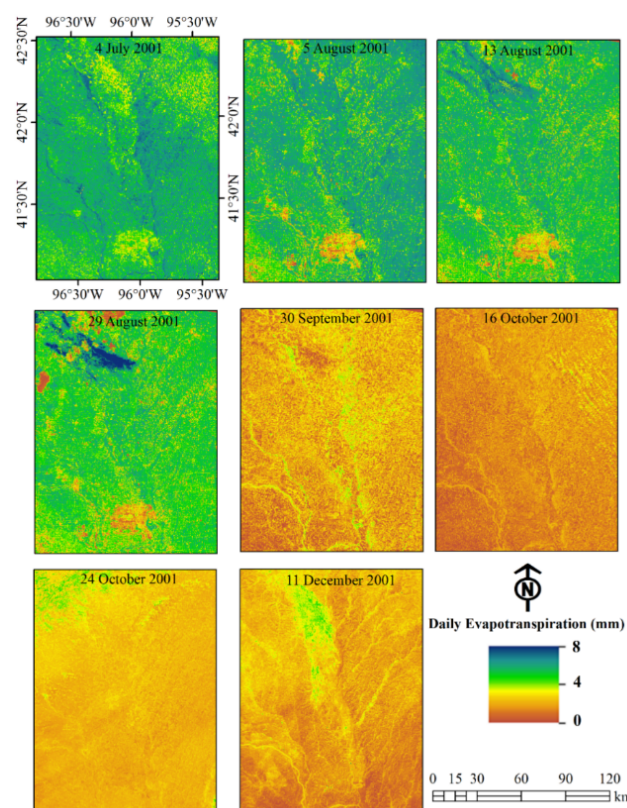

Figure 2. Daily evapotranspiration map for the days of satellite overpasses based on the Mapping EvapoTranspiration at high Resolution with Internalized Calibration (METRIC) model.

Table 2. Evaporation coefficient (K_e) for the hot pixel used in the Mapping EvapoTranspiration at high Resolution with Internalized Calibration (METRIC) model on the date of satellite overpasses.

Date	4 July 2001	5 August 2001	13 August 2001	29 August 2001	30 September 2001	16 October 2001	24 October 2001	11 December 2001
K_e	0.63	0	0	0.31	0.11	0.25	0.62	0.22

3.2. Spatial and Temporal Variation of ET Using the SEBAL Model

The variations of ET both spatially and temporally using the SEBAL model are shown in Figure 3. Overall, the ET values for SEBAL were lower as compared to the METRIC model-based ET values, particularly during the end of the growing season. This is surprising as we used the same hot/dry

and cold/wet pixels (anchor pixels) for both the METRIC and the SEBAL models run for a particular day of satellite overpass. Studies have shown that some uncertainties are introduced in the model output due to subjectivity associated with the selection of anchor pixels [37,38]. However, in our case, lower values of ET of the SEBAL model are not associated with the anchor pixels selection, as we used the same anchor pixels as those used in the METRIC model. Thus, it is most likely that differences in ET estimates between the METRIC and SEBAL models in this study can be attributed to two factors: (1) differences in how ET_rF and EF are computed; and (2) upscaling methods for converting instantaneous ET to daily ET. The ET_rF in the METRIC model is computed based on instantaneous ET and reference ET at the time of satellite overpass (Equation (3)). Thus, weather observations (temperature, humidity, wind speed, and solar radiation) from the nearby automated weather station are used to tie down the METRIC model output. On the other hand, EF in the SEBAL model is solely based on the instantaneous latent heat, soil heat, and sensible heat fluxes (Equation (5)). In addition, any advection effect cannot be accounted for in the SEBAL model but it is accounted for to some extent in the METRIC model due to use of weather data in ET_r [36]. Furthermore, instantaneous ET is upscaled using daily reference ET (Equation (4)) in the METRIC model, whereas upscaling is done using daily average net radiation (Equation (7)) in the SEBAL model. In this study, we did not use field-measured daily net radiation but computed daily average net radiation based on daily extraterrestrial solar radiation, albedo, and daily atmospheric transmittance. This aspect is further discussed in Sections 3.5 and 3.6.
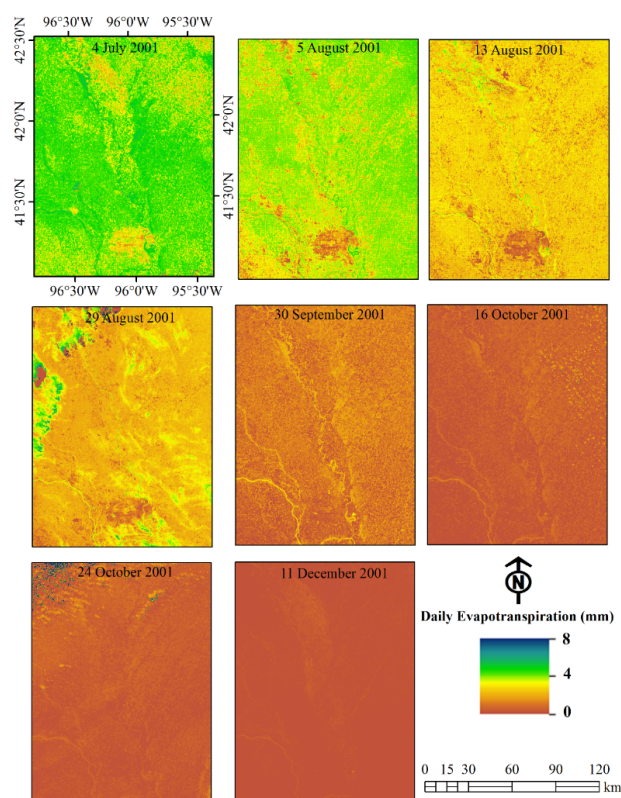

Figure 3. Daily evapotranspiration map for the days of satellite overpasses based on the Surface Energy Balance Algorithm for Land (SEBAL) model.

3.3. Spatial and Temporal Variation of ET Using the SEBS Model

The progression of ET over the study area from July to December was captured by the SEBS model showing good spatial and temporal variations (Figure 4). The transition from high ET values on 4 July 2001 to low ET values on 11 December 2001 was gradual. SEBS showed more variation in

the distribution of ET on the last image date (11 December 2001), than SEBAL ET on 11 December 2001. The ability of the SEBS model to capture the spatial variability has been used in precision agriculture [39]. The ET from the urban area (Omaha, Nebraska) located in the lower middle part of the image is consistent, particularly during July–August. In general, SEBS-estimated ET values were lower than METRIC-estimated ET but higher than SEBAL-estimated ET. However, all three models showed a decreasing trend in ET, as expected with the monthly progression from July to December. It should be noted that daily ET in both SEBAL and SEBS were upscaled using the same daily average net radiation equation ($R_{n24} = (1 - \alpha) \times R_{a24} \times \tau_{sw} - 110 \times \tau_{sw}$) where α is albedo, R_{a24} is daily extraterrestrial solar radiation (W·m^{-2}), and τ_{sw} is daily atmospheric transmittance. However, the spatial distribution of SEBS-based ET was different from SEBAL-based ET, particularly on 13 August, 24 October, and 11 December 2001.
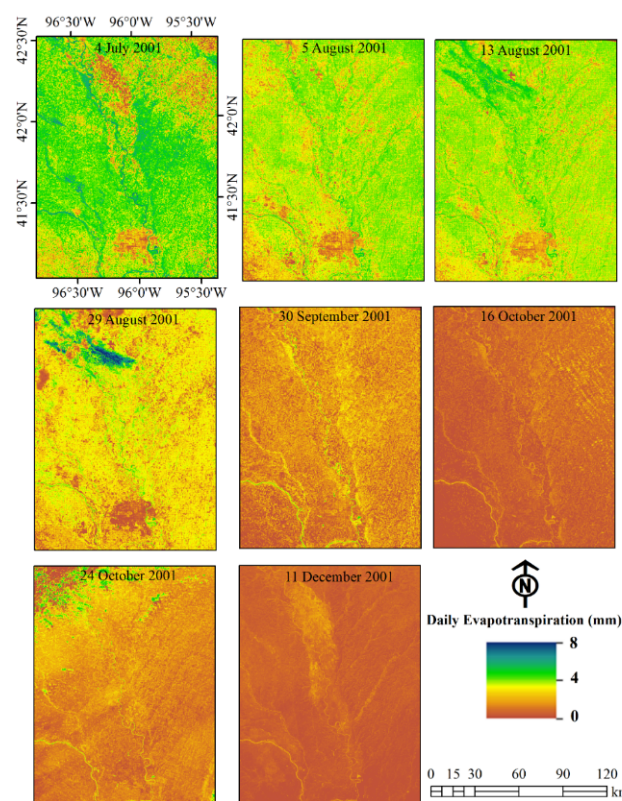

Figure 4. Daily evapotranspiration map for the days of satellite overpasses based on the Surface Energy Balance System (SEBS) model.

3.4. Spatial and Temporal Variation of ET Using the SSEBop Model

Spatial variation and temporal distribution of ET within the study area using the SSEBop model is shown in Figure 5. Unlike METRIC, SEBAL, and SEBS model-based ET, the SSEBop based-ET was the highest for the image acquired on 5 August 2001. This finding was in agreement with the observation that the highest alfalfa reference ET (8.46 mm) among all eight dates was observed on 5 August (Table 3). There were general similarities in ET spatial patterns on 4 July, 5 August, and 13 August 2001 using the METRIC model, whereas different spatial patterns were observed on these dates using the SSEBop model. It should be noted that station-based ET_r was used in the METRIC model for upscaling instantaneous ET to daily ET, whereas Global Data Assimilation System (GDAS)-based short grass reference ET (ET_o) was used in the SSEBop model for computing daily ET. GDAS-based ET_o is a gridded product, thus it captures spatial variability of evaporative demand of the atmosphere better than a single value of ET_r for the entire image. All ET models used in this study showed higher

ET on 24 October as compared to ET on 16 October due to high residual moisture content owing to previous precipitation events (Table 2) and high reference ET (Table 3). However, SSEBop-based ET pattern on 24 October was more in agreement with METRIC-based ET as compared to SEBAL-based ET. ET was minimal on 11 December, consistent with other models due to low evaporative demand of the atmosphere during the winter. However, the SEBS model based ET map has higher spatial variability as compared to the SSEBop model-based ET map on 11 December.
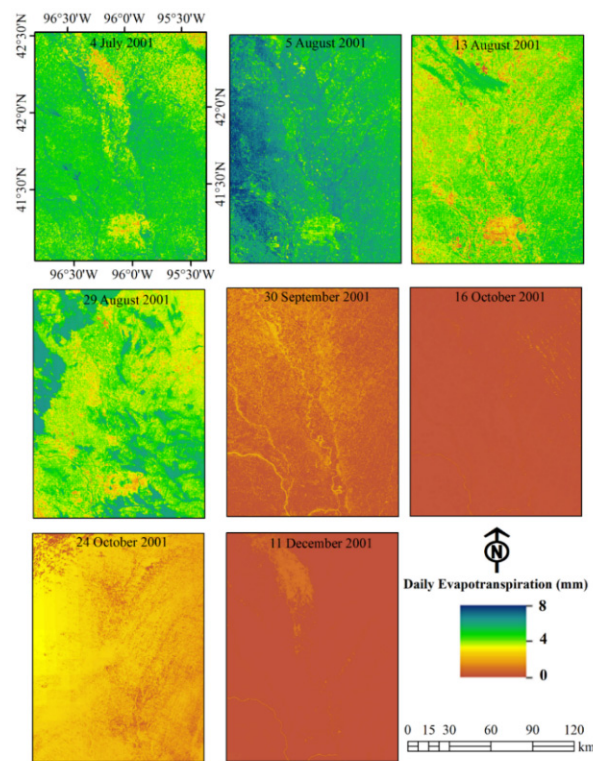

Figure 5. Daily evapotranspiration map for the days of satellite overpasses based on the Operational Simplified Surface Energy Balance (SSEBop) model.

Table 3. Area weighted average (81,921 pixels) short grass reference ET (ET_o) from global data assimilation system and alfalfa reference ET (ET_r) from weather station data for the day of satellite overpasses. Both ET_o and ET_r values are in mm·day^{-1}.

Date	4 July 2001	5 August 2001	13 August 2001	29 August 2001	30 September 2001	16 October 2001	24 October 2001	11 December 2001
ET_o	5.67	6.52	4.82	4.75	2.08	1.35	1.90	0.73
ET_r	6.73	8.46	6.30	7.58	4.49	3.00	3.61	2.66

3.5. Spatial Variation of Evaporative Fraction from Different Models on Selected Dates

As discussed in Section 2, remotely sensed images are first used for computing evaporative fraction at the time of satellite overpass before computing daily ET. The evaporative fraction based on METRIC (ET_rF), SEBAL (EF), SEBS (Λ), and SSEBop (ET_f) models on 4 July 2001 and 5 August 2001 are shown in Figures 6 and 7 respectively. A similar pattern with minor differences was observed for the evaporative fraction within the study area on 4 July 2001 and 5 August 2001 using all four ET models. As compared to ET maps for these two dates using four models (Figures 2–5), there was less variability among evaporative fraction maps (Figures 6 and 7). The urban areas have little lower evaporative fraction on 4 July 2001 using the SEBS model (Figure 6). Similarly, urban areas have little higher evaporative fraction on 5 August 2001 using the SSEBop model (Figure 7).

In general, evaporative fraction is similar to the commonly used crop coefficient approach in crop water requirement computation. Generally, evaporative fraction ranges from 0 to 1 and may be a little higher than 1 for recently watered land either due to irrigation or precipitation for alfalfa or maize crops [2]. The evaporative fraction is mostly expected to be relatively constant during the day of the satellite overpass, thus it is used for upscaling instantaneous ET to daily ET [40–42].
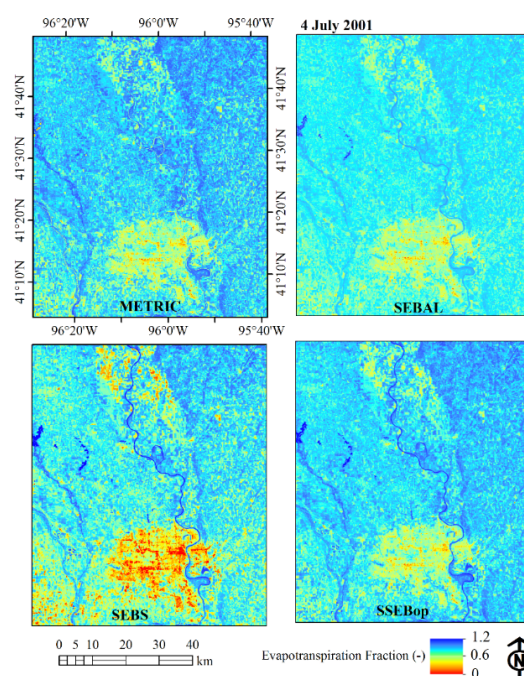

Figure 6. Evaporative fraction map computed using the METRIC, SEBAL, SEBS, and SSEBop models from the Landsat image acquired on 4 July 2001.
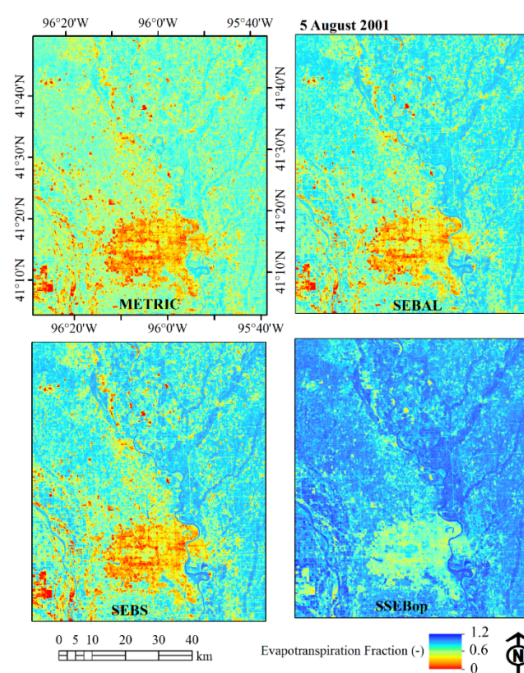

Figure 7. Evaporative fraction map computed using the METRIC, SEBAL, SEBS, and SSEBop models from the Landsat image acquired on 5 August 2001.

3.6. Comparison of Estimated ET with the Eddy Covariance Measurements

Comparison of estimated ET with the field-measured ET gives confidence in the efficacy of any particular model in ET modeling. Our comparison of estimated ET with the measured ET showed that some of the models were effective in tracking the variation of actual ET at all three sites (Figure 8). In general, ET values were relatively higher during the month of July, August, and September and then started to decrease with crop maturity. With the harvest of crops in the second half of October, ET was mostly less than 1 mm·day^{-1}.
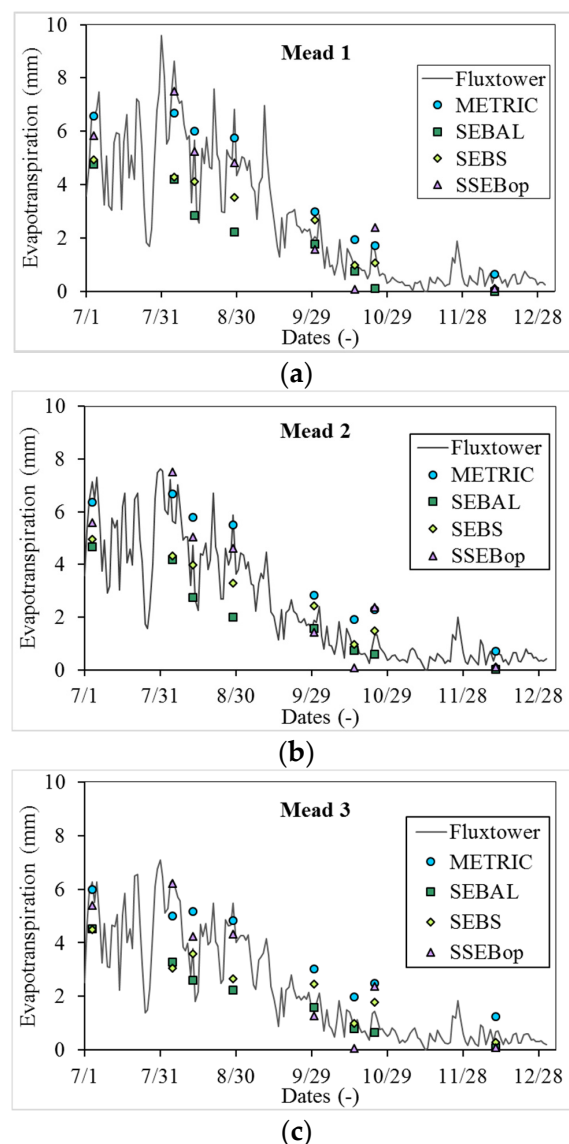

Figure 8. Temporal variation of evapotranspiration measured using eddy covariance at Mead Site 1 (**a**); Mead Site 2 (**b**); and Mead Site 3 (**c**) during 2001. ET estimated using the METRIC, SEBAL, SEBS, and SSEBop models on the days of satellite overpasses are also shown.

Our statistical analysis showed that both the METRIC and SSEBop models performed well at the Mead Sites 1 and 2 with RMSE less than 1 mm·day^{-1} (Table 4). The MAE at the Mead Site 1 ranged from 0.73 mm·day^{-1} (METRIC) to 1.87 mm·day^{-1} (SEBAL) with NSE values of 0.91 and 0.28, respectively. Both SEBAL and SEBS models underestimated ET at the Mead sites. This underestimation was more pronounced, particularly on days of high ET values. This underestimation of ET using

the SEBAL and SEBS models is due to use of an empirical formula of daily average net radiation for upscaling instantaneous ET to daily ET. Our analysis of measured and computed R_{n24} showed that using Equation (7) resulted in good correlation ($r = 0.98$, $R^2 = 0.97$, NSE = 0.65), but there was substantial bias (MBE = -32.17 W·m^{-2}, RMSE = 44.13 W·m^{-2} (34.9%)). Equation (7) worked well when the daily average net radiation values were less than 100 W·m^{-2} but underestimated R_{n24} when the actual R_{n24} was higher than 100 W·m^{-2}. Equation (7) should be calibrated before use to account for local atmospheric conditions. Another study showed the need for improving daily average net radiation estimation for extrapolating instantaneous ET to daily ET [43]. Furthermore, the high uncertainty of the SEBS model due to parameterization errors of roughness length, aerodynamic resistance, and temperature gradient, also has been reported by other researchers [22,44].

The performance of the METRIC model at the dryland Mead Site 3 was not as good as the performance of the SSEBop model. The MAE of the METRIC model at the Mead Site 3 was 0.98 mm·day^{-1} (29.90%), compared to 0.66 mm·day^{-1} (20.26%) for the SSEBop model. The RMSE was 1.06 mm·day^{-1} and 0.73 mm·day^{-1} for the METRIC and SSEBop models, respectively. Similarly, NSE at this site was 0.79 and 0.90 for the METRIC and SSEBop models, respectively. Subdued performance of the METRIC model at the Mead Site 3 may be attributed to the nonirrigated condition of this site. The assumption of constant ET_rF during a day may not be valid under water stressed conditions [2].

Table 4. Comparison statistics for three flux sites based on Pearson's correlation coefficient (r), coefficient of determination (R^2), relative error (RE), mean absolute error (MAE), mean bias error (MBE), root mean square error (RMSE), and Nash–Sutcliffe's efficiency (NSE) using the METRIC, SEBAL, SEBS, and SSEBop models.

Parameters	METRIC Model			SEBAL Model			SEBS Model			SSEBop Model		
	Mead Site 1	Mead Site 2	Mead Site 3	Mead Site 1	Mead Site 2	Mead Site 3	Mead Site 1	Mead Site 2	Mead Site 3	Mead Site 1	Mead Site 2	Mead Site 3
r (-)	0.97	0.97	0.94	0.88	0.93	0.92	0.91	0.94	0.83	0.97	0.95	0.95
R^2 (-)	0.94	0.95	0.88	0.78	0.86	0.85	0.83	0.89	0.68	0.94	0.90	0.91
RE (%)	2.5	11.6	13.7	-47.2	-42.6	-39.6	-31.1	-25.0	-26.0	-12.6	-7.1	-8.1
MAE (mm·day^{-1})	0.73	0.71	0.98	1.87	1.48	1.29	1.48	1.15	1.23	0.74	0.72	0.66
MAE (%)	18.44	19.81	29.90	47.63	41.26	39.59	37.64	31.84	37.60	18.85	20.00	20.26
MBE (mm·day^{-1})	0.10	0.46	0.45	-1.86	-1.67	-1.29	-1.22	-0.96	-0.85	-0.50	-0.22	-0.27
MBE (%)	2.53	12.71	13.71	-47.21	-46.40	-39.59	-31.11	-26.77	-25.99	-12.63	-6.18	-8.15
RMSE (mm·day^{-1})	0.88	0.84	1.06	2.46	2.01	1.74	1.96	1.53	1.67	0.90	0.88	0.73
NSE (-)	0.91	0.90	0.79	0.28	0.42	0.43	0.54	0.66	0.47	0.90	0.89	0.90

3.7. Comparison of Estimated ET for Selected Land Use/Land Cover

Accuracy of different ET products is affected by many factors including the land use/land cover classes [45]. Based on the National Land Cover Database (NLCD) 2001, cropland (77%) and grassland (11%) are the two dominant land cover classes within the study area. The scatterplot of ET for 5 August 2001 estimated using different ET models for cropland shows that there is some degree of linearity for estimated ET, particularly using METRIC, SEBAL, and SEBS models (Figure 9). It can be seen that there is some variation in the scatterplot involving the SSEBop model (Figure 9c,e,f). To understand the source and reason for this variation, we also plotted the scatterplot for evaporative fraction (Figure 10). There was better linearity in evaporative fraction than daily ET computed using all four models, indicating that these models are effectively capturing the instantaneous ET fluxes and evaporative fraction. Thus, more bias in daily ET while upscaling of instantaneous ET to daily ET is caused mainly by different approaches under different ET models used for upscaling.
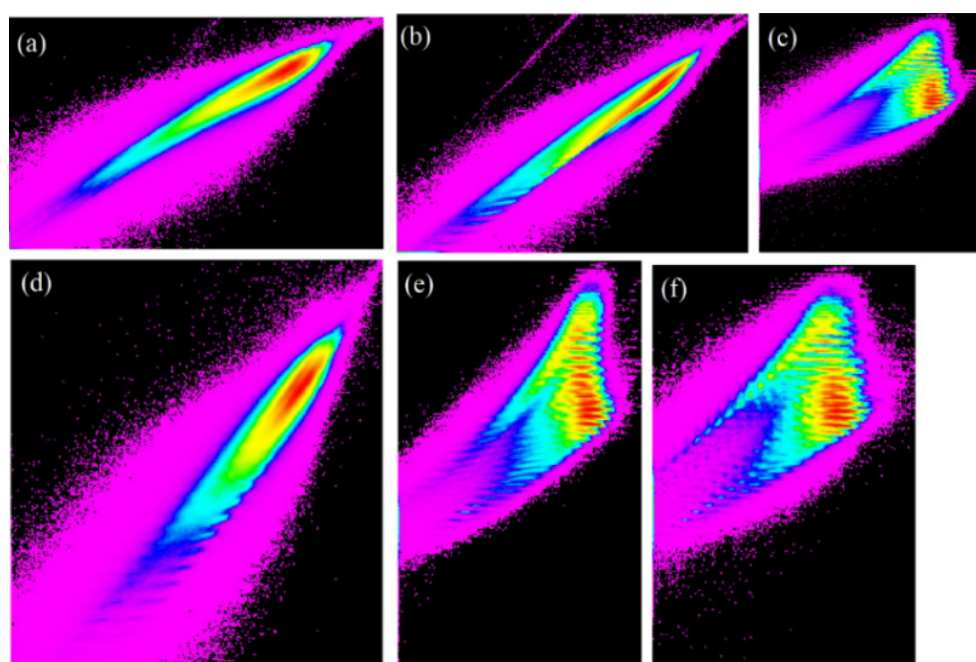
Figure 9. Scatterplot of ET on 5 August 2001 estimated using different ET models for cropland showing (**a**) METRIC model *versus* SEBAL model; (**b**) METRIC model *versus* SEBS model; (**c**) METRIC model *versus* SSEBop model; (**d**) SEBAL model *versus* SEBS model; (**e**) SEBAL model *versus* SSEBop model; and (**f**) SEBS model *versus* SSEBop model. Axes values are ET (mm) such as diagonal line will represent 1:1 line. Different colors in the scatterplots indicate density of points with red being the highest density and magenta being the least density.
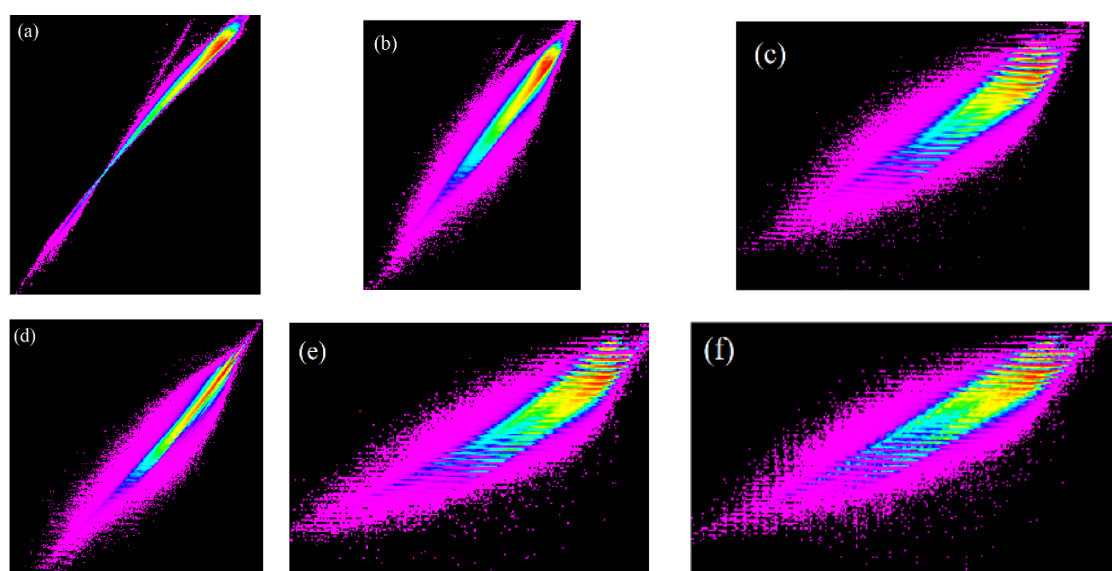

Figure 10. Scatterplot of evaporative fraction estimated for 5 August 2001 using different ET models for cropland showing (**a**) METRIC model (ET_rF) *versus* SEBAL model (*EF*); (**b**) METRIC model (ET_rF) *versus* SEBS model (Λ); (**c**) METRIC model (ET_rF) *versus* SSEBop model (ET_f); (**d**) SEBAL model (*EF*) *versus* SEBS model (Λ); (**e**) SEBAL model (*EF*) *versus* SSEBop model (ET_f); and (**f**) SEBS model (Λ) *versus* SSEBop model (ET_f). Axes values are such as diagonal line represents 1:1 line. Different colors in the scatterplots indicate density of points with red being the highest density and magenta being the least density.

Weather data based on automated weather station were used in the METRIC model for computing ET_r and for upscaling instantaneous ET to daily ET. Thus, the point-based ET_r value is used for the full Landsat image of approximately 170 km north–south by 183 km east–west. Daily average net radiation was used for upscaling instantaneous ET to daily ET for the SEBAL and SEBS model, whereas GDAS-based ET_o was used in the SSEBop model for the same purpose. GDAS-based ET_o is a spatially explicit raster data generated using the standardized Penman–Monteith equation using six-hourly weather datasets [46]. Different methods of upscaling of instantaneous ET to daily ET has its own bias and variation depending upon seasonality and cloud conditions [42].

Similar to cropland ET, the scatterplot of grassland ET also showed some degree of linearity between the METRIC, SEBAL, and SEBS models (Figure 11). However, scatterplots involving the SSEBop model (Figure 11c,e,f) have different distribution patterns from respective scatterplots for cropland (Figure 9c,e,f). We are unable to explain this difference in distribution pattern here and will investigate this discrepancy further in future research.

Similar to cropland, the linearity was even stronger for evaporative fraction of grassland computed using the METRIC, SEBAL, and SEBS models (Figure 12). The scatterplot of the SSEBop model with the other models for grassland also showed a spread-out distribution for ET but not for evaporative fraction. There was good linearity of evaporative fraction computed from all four models for grassland (Figure 12), which indicates that all four ET models used in this study are capturing the spatial variability of instantaneous ET and evaporative fraction for grassland despite differences in model structure. This is most likely due to use of thermal data as the main driving factor in estimating ET using the energy balance approach. Good performance of the METRIC, SEBAL, SEBS, and SSEBop models for estimating ET in grassland are reported in the literature [22,45,47].
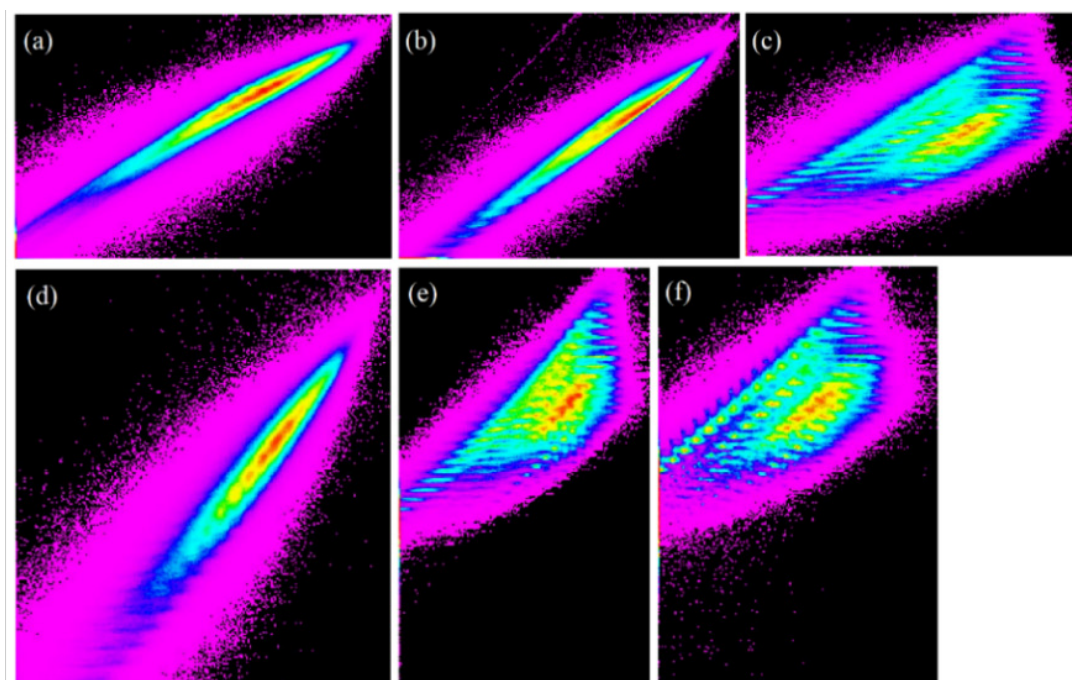

Figure 11. Scatterplot of ET on 5 August 2001 estimated using different ET models for grassland showing (**a**) METRIC model *versus* SEBAL model; (**b**) METRIC model *versus* SEBS model; (**c**) METRIC model *versus* SSEBop model; (**d**) SEBAL model *versus* SEBS model; (**e**) SEBAL model *versus* SSEBop model; and (**f**) SEBS model *versus* SSEBop model. Axes values are ET (mm) such as diagonal line will represent 1:1 line. Different colors in the scatterplots indicate density of points with red being the highest density and magenta being the least density.
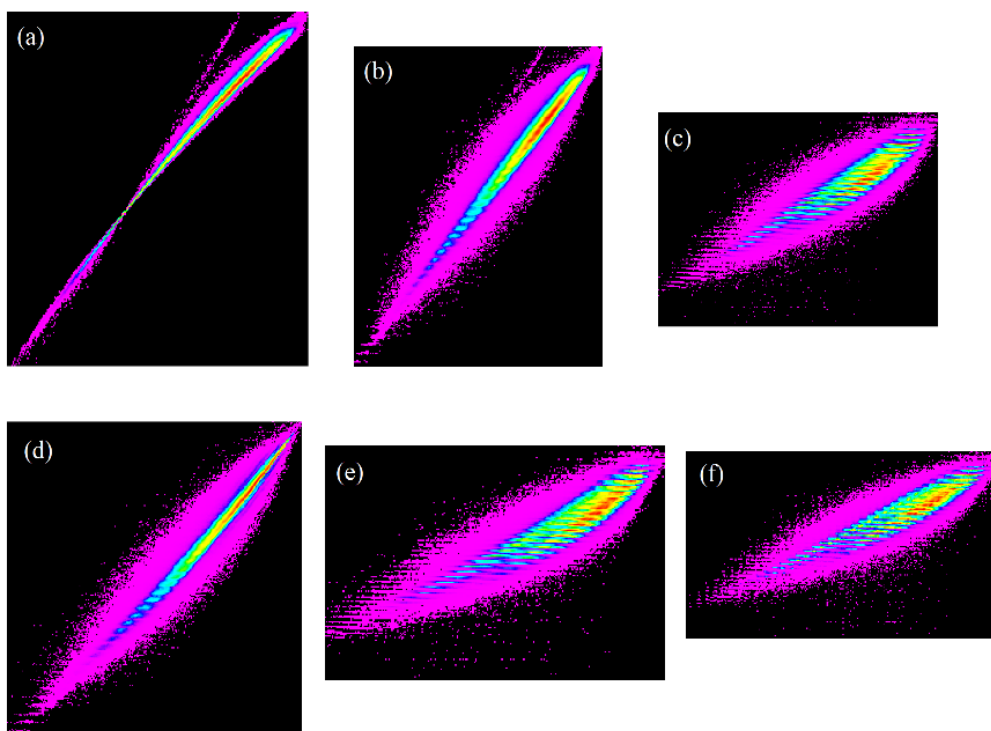
Figure 12. Scatterplot of evaporative fraction estimated for 5 August 2001 using different ET models for grassland showing (**a**) METRIC model (ET_rF) *versus* SEBAL model (*EF*); (**b**) METRIC model (ET_rF) *versus* SEBS model (Λ), (**c**) METRIC model (ET_rF) *versus* SSEBop model (ET_f); (**d**) SEBAL model (*EF*) *versus* SEBS model (Λ); (**e**) SEBAL model (*EF*) *versus* SSEBop model (ET_f); and (**f**) SEBS model (Λ) *versus* SSEBop model (ET_f). Axes values are such as diagonal line represents 1:1 line. Different colors in the scatterplots indicate density of points with red being the highest density and magenta being the least density.

4. Conclusions

Remotely sensed images are increasingly used for quantifying water use at the watershed and larger scale based on different models. Performance of ET models varies depending upon many factors including but not limited to model structure, input data, and user expertise. It is challenging for users to select a particular model from the many that are available to model ET under a given set of circumstances. In this study, four ET models—METRIC, SEBAL, SEBS, and SSEBop—were evaluated using Landsat images over three flux tower sites in the Midwestern United States. Out of three sites, two sites were irrigated maize and one site was dryland maize during 2001.

Though the METRIC, SEBAL, SEBS, and SSEBop models have different degrees of complexity, all four models performed reasonably well in estimating instantaneous ET and evaporative fractions. Even though these four models use different approaches for estimating evaporative fraction, there was some degree of linearity in estimated evaporative fraction. The METRIC model (the most complex among the four tested models) and the SSEBop model (the least complex among the four tested models) resulted in overall comparable performance in estimating ET. Combining data from three flux sites showed that r, R^2, RE, MAE, MBE, RMSE, and NSE values were 0.96, 0.92, 8.9%, 22.52%, 8.93%, 0.93 mm, and 0.80, respectively, for the METRIC model; and were 0.96, 0.92, −9.4%, 20.23%, −9.43%, 0.84 mm, and 0.84, respectively, for the SSEBop model. This finding indicates that added complexity does not necessarily lead to improved model performance, as reported by other researchers [28].

While using the SEBAL and SEBS models, users should be careful in upscaling the instantaneous ET to daily ET. Commonly used upscaling approaches based on the empirical equation of daily average net radiation may not work particularly if there is any cloudiness during, before, or after the time of the

satellite overpass. In addition, local climatic and atmospheric conditions must be accounted for in any daily average net radiation computation for accurate estimation of daily ET. Under these circumstances, users should either use ground-based daily average net radiation measurements or locally recalibrate Equation (7) using theoretical extraterrestrial solar radiation and standard atmospheric transmissivity for computing daily average net radiation. Our study provides some evidence on the usefulness and limitations of these four ET models for accurate quantification of ET, which can help modelers improve the model and help model users select the right model for estimating ET over agricultural areas.

Author Contributions: R.K.S co-developed the study design, collected the data, coded and ran the models, analyzed the models results, carried out statistical analysis, and wrote the manuscript. G.B.S co-developed the study design, helped with the data analysis and interpretations, and edited several draft of the manuscript.

Conflicts of Interest: The authors declare no conflict of interest.

References

1. Pereira, L.S.; Allen, R.G.; Smith, M.; Raes, D. Crop evapotranspiration estimation with FAO56: Past and future. *Agric. Water Manag.* **2015**, *147*, 4–20. [CrossRef]
2. Allen, R.; Irmak, A.; Trezza, R.; Hendrickx, J.M.H.; Bastiaanssen, W.; Kjaersgaard, J. Satellite-based ET estimation in agriculture using SEBAL and METRIC. *Hydrol. Process.* **2011**, *25*, 4011–4027. [CrossRef]
3. Yan, H.; Wang, S.Q.; Billesbach, D.; Oechel, W.; Bohrer, G.; Meyers, T.; Martin, T.A.; Matamala, R.; Phillips, R.P.; Rahman, F.; *et al.* Improved global simulations of gross primary product based on a new definition of water stress factor and a separate treatment of C3 and C4 plants. *Ecol. Model.* **2015**, *297*, 42–59. [CrossRef]
4. Vicente-Serrano, S.M.; Camarero, J.J.; Zabalza, J.; Sanguesa-Barreda, G.; Lopez-Moreno, J.I.; Tague, C.L. Evapotranspiration deficit controls net primary production and growth of silver fir: Implications for Circum-Mediterranean forests under forecasted warmer and drier conditions. *Agric. For. Meteorol.* **2015**, *206*, 45–54. [CrossRef]
5. Karlsson, I.B.; Sonnenborg, T.O.; Seaby, L.P.; Jensen, K.H.; Refsgaard, J.C. Effect of a high-end CO_2-emission scenario on hydrology. *Clim. Res.* **2015**, *64*, 39–54. [CrossRef]
6. Anderson, M.C.; hain, C.; Otkin, J.; Zhan, X.; Mo, K.; Svoboda, M.; Wardlow, B.; Pimstein, A. An intercomparison of drought indicators based on thermal remote sensing and NLDAS-2 simulations with U.S. drought monitor classifications. *J. Hydrometeorol.* **2013**, *14*, 1035–1056. [CrossRef]
7. Yimam, Y.T.; Ochsner, T.E.; Kakani, V.G. Evapotranspiration partitioning and water use efficiency of switchgrass and biomass sorghum managed for biofuel. *Agric. Water Manag.* **2015**, *155*, 40–47. [CrossRef]
8. Spies, R.R.; Franz, K.J.; Hogue, T.S.; Bowman, A.L. Distributed hydrologic modeling using satellite-derived potential evapotranspiration. *J. Hydrometeorol.* **2015**, *16*, 129–146. [CrossRef]
9. Snyder, R.L.; Pedras, C.; Montazar, A.; Henry, J.M.; Ackley, D. Advances in ET-based landscape irrigation management. *Agric. Water Manag.* **2015**, *147*, 187–197. [CrossRef]
10. Nolan, R.H.; Lane, P.N.J.; Benyon, R.G.; Bradstock, R.A.; Mitchell, P.J. Trends in evapotranspiration and streamflow following wildfire in resprouting eucalypt forests. *J. Hydrol.* **2015**, *524*, 614–624. [CrossRef]
11. Bastiaanssen, W.G.M.; Karimi, P.; Rebelo, L.M.; Duan, Z.; Senay, G.; Muthuwatte, L.; Smakhtin, V. Earth observation based assessment of the water production and water consumption of Nile Basin agro-ecosystems. *Remote Sens.* **2014**, *6*, 10306–10334. [CrossRef]
12. Gowda, P.H.; Chavez, J.L.; Colaizzi, P.D.; Evett, S.R.; Howell, T.A.; Tolk, J.A. ET mapping for agricultural water management: Present status and challenges. *Irrig. Sci.* **2008**, *26*, 223–237. [CrossRef]
13. Glenn, E.P.; Nagler, P.L.; Huete, A.R. Vegetation Index Methods for estimating evapotranspiration by remote sensing. *Surv. Geophys.* **2010**, *31*, 531–555. [CrossRef]
14. Kalma, J.D.; McVicar, T.R.; McCabe, M.F. Estimating land surface evaporation: A review of methods using remotely sensed surface temperature data. *Surv. Geophys.* **2008**, *29*, 421–469. [CrossRef]

15. Bastiaanssen, W.G.M. *Regionalization of Surface Flux Densities and Moisture Indicators in Composite Terrain: A Remote Sensing Approach under Clear Skies in Mediterranean Climates*; Report 109; DLO The Winand Staring Centre: Wageningen, The Netherlands, 1995.

16. Bastiaanssen, W.G.M.; Menenti, M.; Feddes, R.A.; Holtslag, A.A.M. A remote sensing surface energy balance algorithm for land (SEBAL)—1. Formulation. *J. Hydrol.* **1998**, *212*, 198–212. [CrossRef]

17. Su, Z. The Surface Energy Balance System (SEBS) for estimation of turbulent heat fluxes. *Hydrol. Earth Syst. Sci.* **2002**, *6*, 85–99. [CrossRef]

18. Allen, R.G.; Tasumi, M.; Trezza, R. Satellite-based energy balance for mapping evapotranspiration with internalized calibration (METRIC)—Model. *J. Irrig. Drain. Eng.* **2007**, *133*, 380–394. [CrossRef]

19. Senay, G.B.; Bohms, S.; Singh, R.K.; Gowda, P.H.; Velpuri, N.M.; Alemu, H.; Verdin, J.P. Operational evapotranspiration mapping using remote sensing and weather datasets: A new parameterization for the SSEB approach. *J. Am. Water Resour. Assoc.* **2013**, *49*, 577–591. [CrossRef]

20. Singh, R.; Senay, G.; Velpuri, N.; Bohms, S.; Scott, R.; Verdin, J. Actual evapotranspiration (water use) assessment of the Colorado River Basin at the Landsat resolution using the Operational Simplified Surface Energy Balance Model. *Remote Sens.* **2013**, *6*, 233–256. [CrossRef]

21. Bastiaanssen, W.G.M.; Noordman, E.J.M.; Pelgrum, H.; Davids, G.; Thoreson, B.P.; Allen, R.G. SEBAL model with remotely sensed data to improve water-resources management under actual field conditions. *J. Irrig. Drain. Eng.* **2005**, *131*, 85–93. [CrossRef]

22. Ershadi, A.; McCabe, M.F.; Evans, J.P.; Chaney, N.W.; Wood, E.F. Multi-site evaluation of terrestrial evaporation models using FLUXNET data. *Agric. For. Meteorol.* **2014**, *187*, 46–61. [CrossRef]

23. French, A.N.; Hunsaker, D.J.; Thorp, K.R. Remote sensing of evapotranspiration over cotton using the TSEB and METRIC energy balance models. *Remote Sens. Environ.* **2015**, *158*, 281–294. [CrossRef]

24. Irmak, S.; Istanbulluoglu, E.; Irmak, A. An evaluation of evapotranspiration model complexity against performance in comparison with Bowen ratio energy balance measurements. *Trans. ASABE* **2008**, *51*, 1295–1310. [CrossRef]

25. Li, S.; Zhang, L.; Kang, S.; Tong, L.; Du, T.; Hao, X.; Zhao, P. Comparison of several surface resistance models for estimating crop evapotranspiration over the entire growing season in arid regions. *Agric. For. Meteorol.* **2015**, *208*, 1–15. [CrossRef]

26. Lu, J.; Sun, G.; McNulty, S.G.; Amatya, D.M. A comparison of six potential evapotranspiration methods for regional use in the southeastern United States. *J. Am. Water Resour. Assoc.* **2005**, *41*, 621–633. [CrossRef]

27. Gonzalez-Dugo, M.P.; Neale, C.M.U.; Mateos, L.; Kustas, W.P.; Prueger, J.H.; Anderson, M.C.; Li, F. A comparison of operational remote sensing-based models for estimating crop evapotranspiration. *Agric. For. Meteorol.* **2009**, *149*, 1843–1853. [CrossRef]

28. Orth, R.; Staudinger, M.; Seneviratne, S.I.; Seibert, J.; Zappa, M. Does model performance improve with complexity? A case study with three hydrological models. *J. Hydrol.* **2015**, *523*, 147–159. [CrossRef]

29. El Tahir, M.E.H.; Wenzhong, W.; Xu, C.Y.; Youjing, Z.; Singh, V.P. Comparison of methods for estimation of regional actual evapotranspiration in data scarce regions: Blue Nile Region, Eastern Sudan. *J. Hydrol. Eng.* **2012**, *17*, 578–589. [CrossRef]

30. Wilson, K.B.; Hanson, P.J.; Mulholland, P.J.; Baldocchi, D.D.; Wullschleger, S.D. A comparison of methods for determining forest evapotranspiration and its components: Sap-flow, soil water budget, eddy covariance and catchment water balance. *Agric. For. Meteorol.* **2001**, *106*, 153–168. [CrossRef]

31. Consoli, S.; Vanella, D. Comparisons of satellite-based models for estimating evapotranspiration fluxes. *J. Hydrol.* **2014**, *513*, 475–489. [CrossRef]

32. Chen, Y.; Xia, J.; Liang, S.; Feng, J.; Fisher, J.B.; Li, X.; Li, X.; Liu, S.; Ma, Z.; Miyata, A.; *et al.* Comparison of satellite-based evapotranspiration models over terrestrial ecosystems in China. *Remote Sens. Environ.* **2014**, *140*, 279–293. [CrossRef]

33. Verma, S.B.; Dobermann, A.; Cassman, K.G.; Walters, D.T.; Knops, J.M.; Arkebauer, T.J.; Suyker, A.E.; Burba, G.G.; Amos, B.; Yang, H.; *et al.* Annual carbon dioxide exchange in irrigated and rainfed maize-based agroecosystems. *Agric. For. Meteorol.* **2005**, *131*, 77–96. [CrossRef]

34. Su, H.; McCabe, M.F.; Wood, E.F.; Su, Z.; Prueger, J.H. Modeling evapotranspiration during SMACEX: Comparing two approaches for local- and regional-scale prediction. *J. Hydrometeorol.* **2005**, *6*, 910–922. [CrossRef]

35. Foken, T.; Aubinet, M.; Finnigan, J.J.; Leclerc, M.Y.; Mauder, M.; Paw, U.K.T. Results of a panel discussion about the energy balance closure correction for trace gases. *Bull. Am. Meteorol. Soc.* **2011**, *92*. [CrossRef]

36. Singh, R.K.; Irmak, A. Treatment of anchor pixels in the METRIC model for improved estimation of sensible and latent heat fluxes. *Hydrol. Sci. J.* **2011**, *56*, 895–906. [CrossRef]

37. Long, D.; Singh, V.P. Assessing the impact of end-member selection on the accuracy of satellite-based spatial variability models for actual evapotranspiration estimation. *Water Resour. Res.* **2013**, *49*, 2601–2618. [CrossRef]

38. Paul, G.; Gowda, P.H.; Vara Prasad, P.V.; Howell, T.A.; Staggenborg, S.A.; Neale, C.M.U. Lysimetric evaluation of SEBAL using high resolution airborne imagery from BEAREX08. *Adv. Water Resour.* **2013**, *59*, 157–168. [CrossRef]

39. Mahour, M.; Stein, A.; Sharifi, A.; Tolpekin, V. Integrating super resolution mapping and SEBS modeling for evapotranspiration mapping at the field scale. *Precis. Agric.* **2015**, *16*, 571–586. [CrossRef]

40. Chavez, J.L.; Neale, C.M.U.; Prueger, J.H.; Kustas, W.P. Daily evapotranspiration estimates from extrapolating instantaneous airborne remote sensing ET values. *Irrig. Sci.* **2008**, *27*, 67–83. [CrossRef]

41. Colaizzi, P.D.; Evett, S.R.; Howell, T.; Tolk, J.A. Comparison of five models to scale daily evapotranspiration from one-time-of-day measurements. *Trans. Am. Soc. Agric. Eng.* **2006**, *49*, 1409–1419. [CrossRef]

42. Cammalleri, C.; Anderson, M.C.; Kustas, W.P. Upscaling of evapotranspiration fluxes from instantaneous to daytime scales for thermal remote sensing applications. *Hydrol. Earth Syst. Sci.* **2014**, *18*, 1885–1894. [CrossRef]

43. Zhang, X.C.; Wu, J.W.; Wu, H.Y.; Chen, H.R.; Zhang, T. Improving temporal extrapolation for daily evapotranspiration using radiation measurements. *J. Appl. Remote Sens.* **2013**, *7*. [CrossRef]

44. Timmermans, J.; Su, Z.; van der Tol, C.; Verhoef, A.; Verhoef, W. Quantifying the uncertainty in estimates of surface-atmosphere fluxes through joint evaluation of the SEBS and SCOPE models. *Hydrol. Earth Syst. Sci.* **2013**, *17*, 1561–1573. [CrossRef]

45. Velpuri, N.M.; Senay, G.B.; Singh, R.K.; Bohms, S.; Verdin, J.P. A comprehensive evaluation of two MODIS evapotranspiration products over the conterminous United States: Using point and gridded FLUXNET and water balance ET. *Remote Sens. Environ.* **2013**, *139*, 35–49. [CrossRef]

46. Senay, G.B.; Verdin, J.P.; Lietzow, R.; Melesse, A.M. Global daily reference evapotranspiration modeling and evaluation. *J. Am. Water Resour. Assoc.* **2008**, *44*, 969–979. [CrossRef]

47. Timmermans, W.J.; Kustas, W.P.; Anderson, M.C.; French, A.N. An intercomparison of the surface energy balance algorithm for land (SEBAL) and the two-source energy balance (TSEB) modeling schemes. *Remote Sens. Environ.* **2007**, *108*, 369–384. [CrossRef]